Resonance interference and absolute cross sections in near-threshold electron-impact excitation of the $3s^2\ ^1S \rightarrow 3s3p\ ^3P$ and $3s^2\ ^1S \rightarrow 3s3p\ ^1P$ transitions in Ar^{6+}

Y-S. Chung, N. Djurić, B. Wallbank,* and G. H. Dunn†
JILA, National Institute of Standards and Technology and the University of Colorado, Boulder, Colorado 80309-0440

M. E. Bannister
Physics Division, Oak Ridge National Laboratory, Oak Ridge, Tennessee 37831-6372

A. C. H. Smith
University College London, London WC1E 6BT, United Kingdom
(Received 3 September 1996)

Strong resonance features were observed in the near-threshold excitation of Ar^{6+}. Absolute total cross sections for electron-impact excitation of the $3s^2\ ^1S \rightarrow 3s3p\ ^3P^o$ and $3s^2\ ^1S \rightarrow 3s3p\ ^1P^o$ transitions in Ar^{6+} were measured by using the merged electron-ion beams energy loss technique. The results are compared with the *R*-matrix close-coupling theory (CCR) and the independent-process isolated-resonance distorted-wave approximation. Observed disagreement between CCR theory and experiment at the near-threshold peak for the $3s^2\ ^1S \rightarrow 3s3p\ ^3P^o$ transition is interpreted to be due to very sensitive resonance interference. [S1050-2947(97)05603-5]

PACS number(s): 34.80.Kw

I. INTRODUCTION

Modeling and diagnostics of nonequilibrium plasmas require cross sections for the multitude of collision processes that occur. In hot plasmas electron-ion collisions are of particular importance. Thus, it has long been a goal [1] of fusion physicists [2], astrophysicists, and others concerned with these plasmas to obtain reliable cross sections. Physicists have responded by developing theoretical methods to produce cross sections, and with modern computers they are able to generate vast quantities of the required data. The huge effort of the Opacity Project is one prominent recent example [3]. Accompanying this theoretical endeavor, for more than thirty years there has been synergistic effort by experimental physicists to measure a reasonable number of cross sections to test the theoretical results. This paper is of that nature, and, unusually when compared to other experimental measurements of electron-ion excitation, reports observations of resonances and the implications of interferences of the resonances.

In the specific case of electron-impact excitation, tens of thousands of cross sections are available from the theoretical work. They frequently exhibit the striking characteristic that numerous resonances are present — one can get the impression of a forest of resonances from looking at plots of the cross sections. These calculated resonances often significantly influence the cross section averaged over an energy distribution, and thus also rate coefficients in a plasma. The relative importance of resonances is frequently amplified for nondipole transitions. Such resonances are a feature of the Coulomb field, and closely related resonances are also found in cross sections for electron-ion ionization [4] and dielectronic recombination [5]. It is significant that most of the experimental excitation results [6] to date either have not shown resonance structure or have presented weak tests of the resonance theory.

Influenced by theoretical calculations [7] on Kr^{6+}, which showed strong resonance structure near the excitation threshold, we conducted earlier experimental measurements [8] on that species and did indeed observe robust resonance features. However, the data did not match the original theoretical calculations, and it was only after additional effects were included that the calculations [9] were brought into line with our experimental results. This, for the first time, confirmed experimentally an important point that Griffin *et al.* [10] had made: that there is extreme sensitivity of the interference of resonances to the exact energies of the resonances, and caution should be exercised in using theoretical results with such resonances. However, as Gorczyca *et al.* [9] pointed out, the Kr^{6+} calculations were complicated by the existence of a full $3d$ shell and by the fact that relativistic operators are responsible for roughly 1-eV shifts in the relative target energies. Also, there is a 1-eV fine-structure splitting between $4s4p(^3P_{0,1,2})$ levels, necessitating a Breit-Pauli treatment of the target states. Such complications made it unlikely that one could expect ready convergence of experiment and theory.

It was thus clear that other less complicated examples of resonances should be examined experimentally and compared with theory to determine the extent of resonance interference. Again guided by indications of theory [11,12], the present work on Ar^{6+} was undertaken with this goal in mind. Strong dielectronic resonances near threshold are predicted by theory for the transition $3s^2\ ^1S \rightarrow 3s3p\ ^3P^o$, and this intercombination excitation is examined as well as the dipole-allowed $3s^2\ ^1S \rightarrow 3s3p\ ^1P^o$ excitation.

*Permanent address: Department of Physics, St. Francis Xavier University, Antigonish, Nova Scotia, Canada B2G 2W5.

†Quantum Physics Division, National Institute of Standards and Technology.

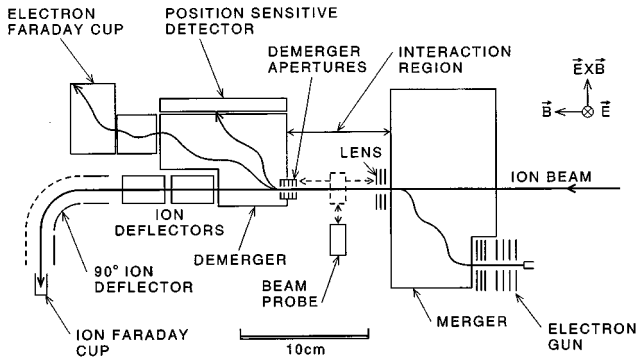

FIG. 1. Schematic view of the merged electron-ion beam energy loss (MEIBEL) apparatus.

II. THE EXPERIMENT

General

We have used the JILA-ORNL merged electron-ion beams energy loss (MEIBEL) technique. Compared with the crossed beams fluorescence technique by which most absolute measurements of electron-impact excitation of positive ions have been obtained [6,13], MEIBEL has a number of advantages. The detection sensitivity is a factor of 10^3 (or more) greater, the electron energy distribution is narrower, and one can observe not only dipole transitions but also nondipole transitions. The latter features are especially important for the present work on resonances in Ar^{6+} excitation.

Detailed descriptions of the MEIBEL technique and apparatus have been given previously [14], so we provide only an overview here, along with describing improvements and changes made since the earlier reports. A schematic diagram of the experimental setup is shown in Fig. 1.

The portion of the apparatus shown in Fig. 1 is immersed in a uniform magnetic field ($\sim$3 mT). Electrons from the electron gun enter a region of crossed **E** and **B** fields, which is a trochoidal analyzer called the merger. Here the electrons performed two cyclotron orbits while undergoing an $\mathbf{E}\times\mathbf{B}$ drift, so that upon exiting the merger the electrons have the same vectorial velocity as when they entered but their trajectory has been moved perpendicular to the entering axis. Along the exiting axis, the electrons merge with an Ar^{6+} ion beam from an electron-cyclotron resonance (ECR) ion source. The two beams are essentially collinear in the interaction region, an electric field free region about 63.5 mm long. They then pass through the demerger apertures, after which they enter another trochoidal analyzer (the demerger) that directs the primary electron beam into a Faraday cup collector. Here also, those electrons, which have undergone inelastic collisions, are dispersed onto a position-sensitive detector (PSD) consisting of a pair of microchannel plates and a resistive anode. This separation of particles is based upon the *forward* velocity as compared to the perpendicular drift velocity $\boldsymbol{\rho}=\mathbf{E}\times\mathbf{B}/\mathbf{B}^2$ in the crossed **E** and **B** fields.

This last point necessitates special consideration of particles scattered at an angle, as elastic collisions between the electrons and ions also occur with a large cross section. The demerger apertures (see Fig. 1) block those electrons elastically scattered at angles large enough for detection by the PSD if allowed to pass, i.e., those electrons with residual forward velocity comparable to those which have been inelastically scattered.

Ions are bent through 90° and collected in a Faraday cup. Signal collected at the PSD is accompanied by high backgrounds from both the electron and ion beams due primarily to beam-gas scattering, but with some component due to beam-surface scattering. Both beams are thus chopped in a phased four-way pattern [14]; signals with position and timing information are collected in four separate histogram memories, the data from which are corrected for dead time, analyzed, and used to calculate the cross section. The densities of the two beams, $G(x,y,z)$ and $H(x,y,z)$, are measured at a number (usually seven) of positions along their merge path using a fluorescent video probe [15], and the data are used to compute the beams' mutual overlap and form factor F.

The excitation cross section at interaction energy $E_{\text{c.m.}}$ in the center-of-mass system was calculated from the data using the equation

$$\sigma(E_{\text{c.m.}})=\frac{R}{\varepsilon}\left|\frac{\nu_e\nu_i}{\nu_e-\nu_i}\right|\frac{qe^2}{I_eI_i}F, \tag{1}$$

where R is the signal count rate from detection of inelastically scattered electrons by the PSD, ε the measured PSD detection efficiency, and ν_e, ν_i, I_e, and I_i are the laboratory velocities and currents of electrons and ions of electric charge e and qe, respectively. The form factor F is given by

$$F=\frac{\int G(x,y,z)dx\,dy\int H(x,y,z)dx\,dy}{\int G(x,y,z)H(x,y,z)dx\,dy\,dz}. \tag{2}$$

The count rates registered in separate histogram memories are (1) electron background B_e plus dark background B_d, (2) ion background B_i plus B_d, (3) signal S plus B_e plus B_i plus B_d, and (4) B_d. The background rates are very high compared to S so the corrections for dead time of the channel plates and detector system become very critical as discussed previously [14]. The system as formerly configured was limited by a 3.58-μs dead time primarily coming from the position computer. To improve the ability to take accurate data with less concern for dead time, the system has been reconfigured with a low impedance anode in the PSD, a new position computer [16], and a fast first-in-first-out (FIFO) buffer between the position computer and the histogram memories, giving a net dead time in the strobe channel of 307.0 ± 0.4 ns and in the rate channel of 60.7 ± 0.1 ns. Thus, in this experiment it was possible to measure much higher count rates with significantly less uncertainty in the subtractions of the data channels. This represents the most marked change in the apparatus and technique from that originally described [14].

Procedures and conditions

Typically operating values of the experimental parameters were electron currents of 200 nA, ion currents of 180 nA, form factors around 3×10^{-3} cm, ion energies of 84 and 102 keV, and background pressure in the collision chamber of

2×10^{-8} Pa (1.5×10^{-10} torr). These gave rise to signal rates in the range $S\approx100$–200 s^{-1} accompanied by electron background rates $B_e\approx7000$ s^{-1} and ion background rates $B_i\approx6300$ s^{-1}. Dark rates were on the order of 100 s^{-1}.

The typical data protocol involved tuning the ion and electron beams to achieve minimum backgrounds and to ensure that the beams overlapped reasonably well in front of the demerger apertures and that they did not overlap behind the apertures (so no scattering occurred beyond the demerger apertures). Form factors were then measured. Collection of data in the four channels proceeded at the particular electron energy until adequate statistical uncertainties were reached (usually for on the order of 30 min). The interaction energy was then changed by changing the electron energy. The magnetic field and voltages associated with the electron gun, the merger, and the demerger were carefully scaled by a few percent, and this produced electron beams of near-identical shapes. Thus, form factors could be kept effectively constant and were not measured on subsequent data points until the series of energies was finished, at which time another form factor was taken. If significant change had occurred, the data series was held suspect and discarded. A number of data runs covering the same energy range were made, and averages of three to six measurements at each energy constitute the data presented here (for the 77 data points presented here, there were 288 measurements as described).

Interaction energy

In order to precisely fix the absolute energy scale for the interaction, the measured absolute total excitation cross sections for the Ar^{6+} ($3s^2\ ^1S\rightarrow3s3p\ ^1P^o$) transition were fitted to the convolution of a Gaussian energy distribution of variable width with a step function at 21.17 eV, the spectroscopically determined threshold [17] energy (see Sec. III, Fig. 3). The fitting gives a full width at half maximum (FWHM) interaction-energy spread of 0.24 ± 0.04 eV, where the uncertainty is at the 90% confidence level of the fitting result. A necessary shift in energy was attributed to a ''contact potential'' of about 1.94 V, and this was used for correcting all laboratory electron energies. The FWHM interaction-energy spread was used to determine the width of a Gaussian used to convolute theoretical results in order to compare with experiment.

Ion target purity

Ions from the ECR source are accelerated through a fixed potential, then momentum analyzed so that only particles of fixed $M/q=6.667$ are in the analyzed beam. As there are no other likely impurity species with this M/q, the beam is deemed pure of other nuclear species. However, the $3s3p\ ^3P^o$ state is metastable and there may be a substantial fraction of the ions in this state, thus making a mixed target. The metastable content was measured by routing the (same) ion beam into the ORNL crossed beams apparatus [18] and measuring the apparent ionization cross section of the target ions. The ionization signal observed below the energy threshold for ionizing ground-state ions could be attributed to the metastable ions. Analyzing the resulting data using the algorithm we have used previously [19] yielded the fraction of metastables f_m to be 0.285 ± 0.022. Hence, measured cross sections for excitation from the $3s^2\ ^1S$ ground state had to be corrected by multiplying by $1/(1-fm)=1.399$.

Electron backscattering

It was found in our earlier measurements [20] on Ar^{7+} that near-threshold electrons were inelastically scattered primarily in the backward direction in the center-of-mass system. This was also found theoretically [12] and observed [8,14] for other species. Even on a semiclassical basis, it can be shown [20] that one expects backscattering near threshold for dipole transitions. At the threshold for excitation, the scattered electron has zero velocity in the center-of-mass (c.m.) frame and $V_{\text{c.m.}}$ in the laboratory frame, where $V_{\text{c.m.}}$ is the velocity of the center of mass in the laboratory frame. At energies about threshold, the electron velocity, v_e in the laboratory frame is the vector sum of the velocity v_e' of the scattered electron in the c.m. frame and $V_{\text{c.m.}}$, i.e., $v_e=v_e'\cos\theta'+V_{\text{c.m.}}$, where θ' is the scattering angle in the c.m. system. So scattered electrons move forward into the detector until $v_e'\cos\theta'$ becomes negative and larger in magnetite than $V_{\text{c.m.}}$. Then v_e is negative (the electron moves in the back direction in the laboratory frame) and will not enter the detector. This limits the above threshold energy for which one can make measurements without corrections to the data. Also, at higher scattering energies, scattered electrons with sufficient laboratory velocity perpendicular to the beam axis have large enough cyclotron radii that they may be intercepted by the demerger apertures.

In the present case data were taken at two ion energies as noted earlier. The demerger-detector portion of the apparatus was modeled using a fully three-dimensional trajectory modeling program [21]. To determine needed corrections to the data, the following procedure was used. The beam density information measured with the beam probe was used to determine vertical and horizontal line integrals, thus yielding a two-dimensional density map giving coordinates from which signal electrons would be starting. At the approximate midway position along the merge path, nine positions (center and along two concentric rings) were chosen in this plane for launching test trajectories, and the trajectories were weighted with the line-integral information. Trajectories were launched from each position and at intervals of 10° from 0° to 180°, with trajectories at a given angle weighted by the theoretical differential cross section. For each experimental point needing correction, approximately 1500 trajectories were launched, and the fraction of detector ''hits'' to total launches define the fraction detected and thus determined a correction factor.

Of course, the greater $V_{\text{c.m.}}$ is, the greater the interaction energy can be before any corrections are called for. This is shown in Fig. 2. Figure 2(a) shows the measured cross section for excitation of the $^3P^o$ state at an interaction energy of 14.40 eV. No corrections were necessary, since in both cases $V_{\text{c.m.}}>v_e'$. In Fig. 2(b) the interaction energy is 15.46 eV, and at 84 keV ion energy, $V_{\text{c.m.}}<v_e'$ while at 102 keV $V_{\text{c.m.}}>v_e'$. The square point in this figure represents the

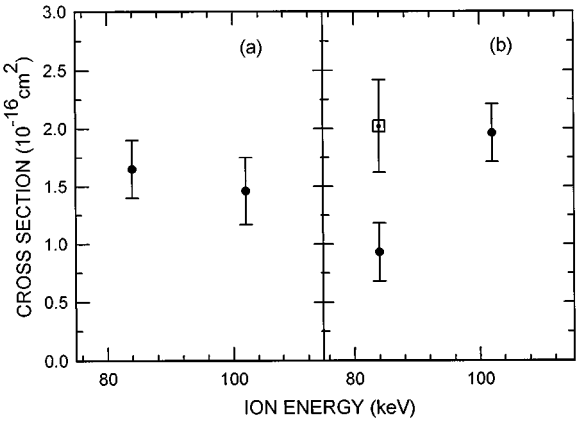

FIG. 2. Cross section for $3s^2\ ^1S \rightarrow 3s3p\ ^3P^o$ transition in electron bombardment of Ar^{6+} measured at two different ion energies (a) $E_{\text{c.m.}}=14.40$ eV; (b) $E_{\text{c.m.}}=15.454$ eV. In (b) the point represented by the square has been corrected for backscattering as discussed in the text.

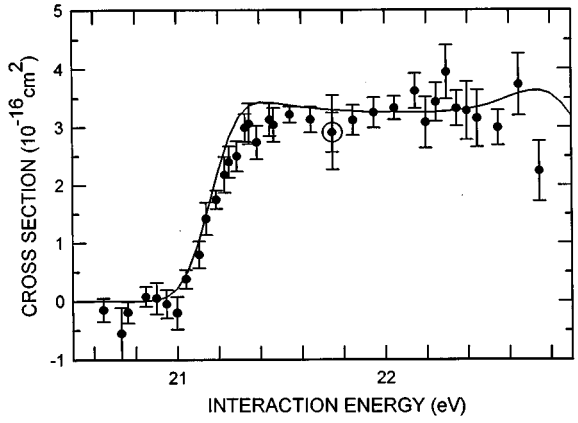

FIG. 3. Cross section vs. center-of-mass interaction energy for electrons bombarding Ar^{6+} and producing the transition $3s^2\ ^1S \rightarrow 3s3p\ ^1P^o$. Points represent average experimental values, and the bars are representative of relative uncertainties at 90% confidence level. The bars on the point at 21.75 eV shown as an open circle represent expanded combined absolute uncertainty U as discussed in the text. The solid curve is a convolution of a Gaussian of width 0.24 eV FWHM with CCR theory from Refs. [12] and [25]. Points above 21.65 eV have been corrected for electron backscattering as discussed in the text.

cross section at 84 keV ion energy after being corrected by the procedure described above, and is seen to agree well with the uncorrected point taken with higher center-of-mass velocity. Using only data taken at 102 keV for the higher interaction energies, it was necessary to make corrections greater than 10% for only about 30% of the points for the $^1P^o$ excitation and less than 7% of the points for the $^3P^o$ excitation. For the $3s^2\ ^1S \rightarrow 3s3p\ ^1P$ transition the correction factors increase from 1 at 21.65 eV to 1.59 at 22.75 eV. For the $3s^2\ ^1S \rightarrow 3s3p\ ^3P$ transition, the correction factor rises from 1 at 15.61 eV to 1.59 at 16.16 eV.

Spurious signals

It is well known that colliding charged-particle-beam experiments [22] are susceptible to a number of sources of unwanted or spurious signals. Thus, background from one beam's hitting a surface (e.g., due to photons or electrons released upon impact) may be modulated by the space charge of the second beam's slightly moving the first beam across the surface. Gas released by one beam's impact on a surface may give rise to a beam-gas background change as the second beam encounters the gas. Beam-beam elastic scattering has already been mentioned. An incorrect value of dead time may give the appearance of a signal when channel subtractions are performed. Finally, it is possible [14] that the target ion beam has a very small fraction of particles in excited states or high Rydberg states which ionize (and thus give off detectable electrons) with an unusually large cross section when an electron collision occurs. It has become routine for us to make extensive tests for these effects in our colliding-beam experiments, the most telling test being the presence or absence of ''signal'' below the energy threshold for the process being examined.

In this experiment, despite extensive tests including appropriate changes of variables, there was a persistent *constant* apparent signal below each threshold investigated that could not be identified. Because it seemed to similar to the background encountered [14] with O^{5+}, it was thought to be most likely due to long-lived autoionizing or high Rydberg states as there. However, the level did not change significantly when changing the ion energy from 102 to 60 keV, giving a 30% change in transit time from the ion source to collision region so that the populations of the rogue states should have changed. Similarly, it did not change when the pressure in the beam transit tube was changed by as much as a factor of 80, nor when slits encountered by the beam in transit to the collision region were substantially opened up. This background was large, being the order of magnitude of the cross section (2×10^{-16} cm^2), but because it was constant, we subtracted it from the data over the relative small energy range from which we report data.

Uncertainties

The relative uncertainties, which have no correlation between data points, are determined by the quadrature sum of uncertainties resulting from counting statistics and uncertainties in the corrections (20% of the correction) for the incomplete collection of signal as determined by the SIMION modeling as described above. Total relative uncertainties are presented at a 90% confidence level. The expanded combined absolute uncertainty [23] U at a similar (90%) level of confidence includes systematic uncertainties, which do not affect the relative shape of the data. Thus, added in quadrature to the relative uncertainties are uncertainties resulting from the metastable content of the ion beam (10%), spatially delimiting the signal on the PSD (3%), spurious signals (12%) [this value does not include an uncertainty in the *assumption* that this background could be subtracted], signal detection efficiency (4%), form factor (10%), and currents (1% each) of the electron and ion beams. Uncertainties in PSD dead time and in the particle velocities were negligible in the scale of other uncertainties. A coverage factor, $k=1.7$, was used to make systematic uncertainties compa-

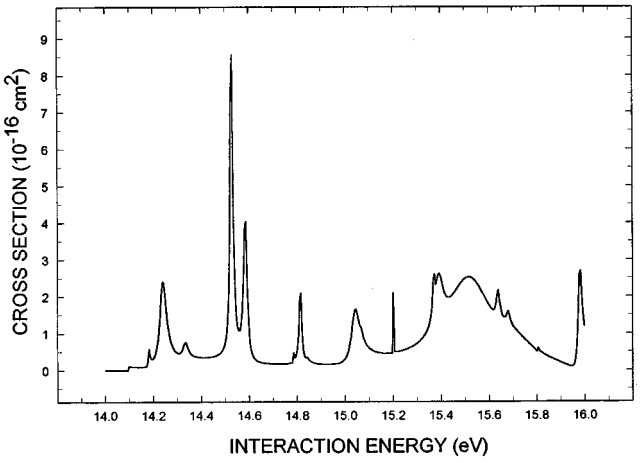

FIG. 4. Theoretical cross section vs center-of-mass interaction energy for electrons bombarding Ar^{6+} and producing the transition $3s^2\ ^1S \rightarrow 3s3p\ ^3P^o$. The curve is adapted from CCR results from Refs. [12] and [25].

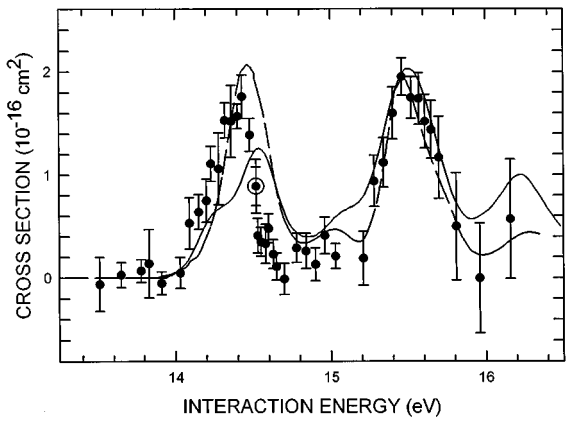

FIG. 5. Cross section vs center-of-mass interaction energy for electrons bombarding Ar^{6+} and producing the transition $3s^2\ ^1S \rightarrow 3s3p\ ^2P^o$. Points are measured and bars are as in Fig. 3. The solid curve is a convolution of a Gaussian (0.24 eV FWHM) with CCR theory from Refs. [12] and [25]. The dashed curve is a similar convolution with IPIRDW approximation theory from the same references.

rable to 90% CL. The typical values of U are 22% (singlet to singlet) and 29% (singlet to triplet).

III. EXPERIMENTAL RESULTS

$3s^2\ ^1S \rightarrow 3s3p\ ^1P^o$

The results for excitation of the dipole-allowed transition are presented [24] graphically in Fig. 3. The solid curve in Fig. 3 represents the R-matrix close coupling (CCR) calculation by Badnell *et al.* [12,25] convoluted with a Gaussian electron energy distribution of 0.24 eV. The bars on the points represent the *relative* uncertainty at 90% confidence level. The point at 21.75 eV with an open circle also shows the *expanded combined absolute uncertainty U* discussed above. As discussed in Sec. II, points above 21.65 eV have been corrected for backscattering.

The good agreement between the experimental values and the convoluted theoretical curve is seen to be within 5–10%, and generally within even relative uncertainties. Here, the direct excitation dominates and there is little opportunity to evaluate resonances in this transition. Though the theory [12] shows a pair of ''high'' resonances near 22.6 and 22.8 eV, they are so narrow that when convoluted with the energy distribution, they produce only the small lump seen between these energies. The experimental data may suggest that this feature is shifted to lower energies, but with the larger uncertainties in this energy region occasioned by the backscattering corrections, it is really possible only to speculate. Since the functional form of the cross section here is rather plain, the data serve well to locate the absolute energy and establish the width of the electron energy distribution.

$3s^2\ ^1S \rightarrow 3s3p\ ^3P^o$

For the $3s^2\ ^1S \rightarrow 3s3p\ ^3P^o$ transition, calculations reveal that quite the opposite is true with respect to the relative importance of resonances. That is, the direct excitation is predicted [12,25] to be from 30 to 100 times smaller than some of the stronger resonances, and the resonances are wide enough that they dominate. This can be seen in Fig. 4 where the unconvoluted results [25] of the CCR (8 state) calculation for this transition are presented.

The experimental results [24] are shown in Fig. 5; the points include relative uncertainties at 90% CL and the expanded combined absolute uncertainty is shown on the point at 14.52 eV. The solid curve represents a convolution of the 0.24 eV FWHM interaction energy distribution with the CCR results shown in Fig. 4. The dashed curve represents a convolution of the energy distribution with results [12,25] of the independent-process isolated-resonance distorted-wave approximation (IPIRDW) approximation. There is not much difference between the two theories nor between the experiment and theories for the resonance near 15.5 eV. However, there is substantial disagreement between the theories for the lower-energy resonance, and quite surprisingly and fortuitously the experiment agrees much more closely with the less sophisticated IPIRDW results.

Each of the major resonances shown in Fig. 5 results from convolution over groups of resonances as can be seen by comparing Figs. 4 and 5. The message of this paper lies in the comparison between the experiment and theory and the efforts of the theorists [25] to investigate the reason for the discrepancies between the CCR calculation and the measurements. They repeated the 8-state CCR calculation a number of times, each time adjusting the separation between the threshold energies of the upper levels of Ar^{6+} to which the strongest of these resonant states are attached. They found that these changes in resonant positions had a relatively small effect on the upper resonances centered about 15.5 eV, but that these variations had a large effect on the lower resonances centered at 14.5 eV. Clearly, the magnitude of these low-lying resonances are sensitive to the interaction between the resonant states and, of course, these interactions are dependent on the separation between resonances. This makes accurate *ab initio* calculations of the resonances contribution to the cross section much more difficult, and demonstrates the importance of additional experimental measurements for such cases.

IV. CONCLUSIONS

Results of this paper emphasize the potential sensitivity of CCR theoretical methods for calculating cross sections for electron-impact excitation of ions when resonances play a strong role in the excitation. The paper underscores the need for continued theoretical effort to find ways to determine resonance locations more accurately in order to improve the correctness of the calculated cross sections. The work also demonstrates the continuing need for close synergism between theory and experiment in the quest for reliable cross sections for modeling of nonequilibrium plasma environments.

ACKNOWLEDGMENTS

The authors wish to thank D. C. Griffin, M. S. Pindzola, J. S. Shaw, and N. R. Badnell for examining resonance as the likely cause of the disagreement between this experiment and theory and for useful discussions. We thank J. W. Hale for skilled technical assistance. This work was supported in part by the Office of Fusion Energy of the U.S. Department of Energy under Contract No. DEA105-86ER53237 with the National Institute of Standards and Technology and Contract No. DEAC05-96OR22464 with Lockheed Martin Energy Research Corp.

[1] See series *Applied Atomic Collision Physics Vol. 1–5* (Academic, London, 1982–84) for five volumes covering applications.

[2] H. P. Summers, in *Advances in Atomic, Molecular and Optical Physics Vol. 33*, edited by M. Inokuti (Academic, New York, 1994), p. 275.

[3] M. J. Seaton, Y. Yu, D. Mihalas, and A. K. Pradhan, Mon. Not. Roy. Astron. Soc. **266**, 805 (1993).

[4] A. Müller, in *Physics of Ion Impact Phenomena*, Springer Series in Chemical Physics Vol. 54, edited by D. Mathur (Springer, Berlin, 1991), pp. 13–90.

[5] *Recombination of Atomic Ions*, Proceedings of NATO Advanced Research Workshop, edited by W. G. Graham *et al.* (Plenum, New York, 1992).

[6] R. A. Phaneuf, in *The Physics of Electronic and Atomic Collisions*, edited by T. Andersen *et al.*, AIP Conf. Proc. No. 295 (AIP, New York, 1993), pp. 405–414.

[7] T. W. Gorczyca, M. S. Pindzola, and D. C. Griffin (private communication).

[8] M. E. Bannister, X. Q. Guo, T. M. Kojima, and G. H. Dunn, Phys. Rev. Lett. **72**, 3336 (1994).

[9] T. Gorczyca, M. S. Pindzola, N. R. Badnell and D. C. Griffin, Phys. Rev. A **51**, 488 (1995).

[10] D. C. Griffin, M. S. Pindzola, F. Robicheaux, T. W. Gorczyca, and N. Badnell, Phys. Rev. Lett. **72**, 3491 (1994). See also: N. R. Badnell, D. C. Griffin, T. W. Gorczyca, and M. S. Pindzola, Phys. Rev. A **48**, R2519 (1993).

[11] N. R. Badnell, D. C. Griffin, T. W. Gorczyca, and M. S. Pindzola, Phys. Rev. A **50**, 1231 (1994).

[12] D. C. Griffin, M. S. Pindzola, and N. R. Badnell, Phys. Rev. A **47**, 2871 (1993).

[13] E. W. Bell, Ph. D. thesis, Univ. Colorado, 1993 (unpublished), available through University Microfilms International (UMI), P.O. Box 1764, Ann Arbor, MI 48106.

[14] E. W. Bell, X. Q. Guo, J. L. Forand, K. Rinn, D. R. Swenson, J. S. Thompson, G. H. Dunn, M. E. Bannister, D. C. Gregory, R. A. Phaneuf, A. C. H. Smith, A. Müller, C. A. Timmer, E. K. Wåhlin, B. D. DePaola, and D. S. Belić, Phys. Rev. A **49**, 4585 (1994).

[15] J. L. Forand, C. A. Timmer, E. K. Wåhlin, B. D. DePaola, G. H. Dunn, D. Swenson, and K. Rinn, Rev. Sci. Instrum. **61**, 3372 (1990).

[16] Quantar Model 2510. This information is given for technical completeness and this is not intended as a product endorsement.

[17] L. W. Phillips and W. L. Parker, Phys. Rev. **60**, 305 (1941).

[18] D. C. Gregory, F. W. Meyer, A. Müller, and P. DeFrance, Phys. Rev. A **34**, 3657, (1986).

[19] N. Djurić, E. W. Bell, X. Q. Guo, G. H. Dunn, R. A. Phaneuf, M. E. Bannister, M. S. Pindzola, and D. C. Griffin, Phys. Rev. A **47**, 4786 (1993).

[20] X. Q. Guo, E. W. Bell, J. S. Thompson, G. H. Dunn, M. E. Bannister, R. A. Phaneuf, and A. C. H. Smith, Phys. Rev. A **47**, R9 (1993).

[21] SIMION 3D Version 6.0; David A. Dahl, Idaho National Engineering Laboratory.

[22] G. H. Dunn, in *Atomic Physics, Vol. I*, edited by B. Bederson, V. W. Cohen, and F. M. J. Pichanick (Plenum, New York, 1969), p. 417.

[23] Uncertainties are presented as per the guidelines in *Guidelines for Evaluating and Expressing the Uncertainty of NIST Measurement Results*, edited by B. N. Taylor and C. E. Kuyatt, NIST Technical Note 1297 (NIST Gaithersburg, 1994).

[24] Tabulated values of the results may be obtained by contacting the authors or by referring to World-Wide Web site http://www-cfadc.phy.ornl.gov/ecrgine/JILA.html.

[25] D. C. Griffin, M. S. Pindzola, J. A. Shaw, N. R. Badnell (private communication).